Proceedings of the ASME 2020 International Technical Conference and Exhibition
on Packaging and Integration of Electronic and Photonic Microsystems
InterPACK2020
October 27-29, 2020, Virtual, Online

IPACK2020-2662

NUMERICAL ANALYSIS OF OIL IMMERSION COOLING OF A SERVER USING MINERAL OIL AND AL2O3 NANOFLUID

Amirreza Niazmand[1], Prajwal Murthy, Satyam Saini, Pardeep Shahi, Pratik Bansode, Dereje Agonafer
The University of Texas at Arlington
Arlington, Texas, USA

ABSTRACT

Increased demand for computer applications has manifested a rise in data generation, resulting in high Power Density and Heat Generation of servers and their components, requiring efficient thermal management. Due to the low heat carrying capacity of air, air cooling is not an efficient method of data center cooling. Hence, the liquid immersion cooling method has emerged as a prominent method, where the server is directly immersed in a dielectric liquid. The thermal conductivity of the dielectric liquids is drastically increased with the introduction of non-metallic nanoparticles of size between 1 to 150 nm, which has proven to be the best method. To maintain the dielectric feature of the liquid, non-metallic nanoparticles can be added.

Alumina nanoparticles with a mean size of 80 nm and a mass concentration of 0 to 5% with mineral oil are used in the present study. The properties of the mixture were calculated based on the theoretical formula and it was a function of temperature. Heat transfer and effect of the nanoparticle concentration on the junction temperature of the processors using CFD techniques were simulated on an open commute server with two processors in a row. The junction temperature was studied for different flow rates of 0.5, 1, 2, and 3 LPM, at inlet temperatures of 25, 35, and 45 degrees Celsius. The chosen heatsink geometries were: Parallel plate, Pin fin, and Plate fin heatsinks.

Keywords: Open commute server, thermal conductivity, specific heat, mass concentration, immersion cooling, CPU temperature, pressure drop, pumping power

NOMENCLATURE

h	heat transfer coefficient
Re	Reynolds Number
Pr	Prandtl's Number
Nu	Nusselt's Number
ΔP	Pressure Drop
W	Watt
LPM	Liter per Minute
Conc	Concentration
Vol	Volume
f	Base fluid
nf	nanofluid
K	Thermal conductivity
μ	viscosity
Ø	Mass concentration of nano particles
β	Fluid expansion ratio
ρ	Density
Cp	Specific heat

INTRODUCTION

The data center is a dedicated space in an industry that houses the servers mounted in racks, where the generated data is stored, managed, and disseminated accordingly. The most critical

[1] Contact author: amirezza.nizamand@mavs.uta.edu

systems of networks are housed in data centers, ensuring the continuity of daily operations. Advancement in technology has resulted in a paradigm shift, with a strong dependency on computer systems and their applications, causing rapid growth in data centers, seen in various areas like IT industries, banking, social media, education, R&D, etc [1],[2]. This ever-increasing demand posits drawbacks, manifested in the increase in power density and heat generation of servers, with considerable energy consumption by the data centers. With an improvement in semiconductor technologies, IT load is expected to increase, necessitating an efficient data center cooling method [3], [4]. The United States Department of Energy in collaboration with Lawrence Berkeley National Laboratory have reported the consumption of 70 billion kWh of energy by data centers in 2014, which represents 2% of the country's total energy consumption, accounting for 40% of the total energy's bill [6],[7]. To maintain the safe operation and reliability of the servers along with the reduction in energy consumption by data centers, there is a need to adopt an energy-efficient data center cooling method. Air cooling is the most commonly used method of data center cooling. It works on the principle of forced convection of air over the heatsink. The heatsink helps in dissipating the generated heat from the server and it's components to the surrounding medium. The airflow is supplied utilizing axial fans, and their speeds are controlled according to the change in temperature of the server and its components. Poor specific heat capacity and thermal conductivity of air have developed a need to increase surface area for enhancing heat transfer, which can be achieved by increasing the number of heatsink fins. This results in the complexity of the system and additional costs. Also, a large space is occupied by the ducting systems and fans. Due to the posed drawbacks, its application in cooling servers, microprocessors, and dense packages have subsided over the years. To overcome these shortcomings, liquid cooling is considered to be a viable alternative for the cooling of data centers and servers. [8], [9].

Water cooling is an indirect method of liquid cooling, with advantages over conventional air cooling such as higher specific heat and lower transport energy requirements that help in more reduction of temperature in the high heat-generating electronic components and dense packages. Cooling occurs through conduction and convective modes of heat transfer using a cold plate, where the base of the cold plate gets heated through conduction, and heat is transferred from the cold plate base to water through convection. However, air cooling is still required for a few components within the server, with additional costs for design and fabrication of cold plates, ducts, plumbing systems, quick disconnects (QD's), controls, and heat exchangers. All liquid systems demand complex cold plate geometries, increasing the cost of operation. Also, the high electric conductivity of water hinders the direct immersion of servers. Hence, immersion cooling is an alternative to water-cooled servers, which involves submerging the server inside a dielectric fluid, which ensures substantial energy savings and low cost of operation [10], [11].

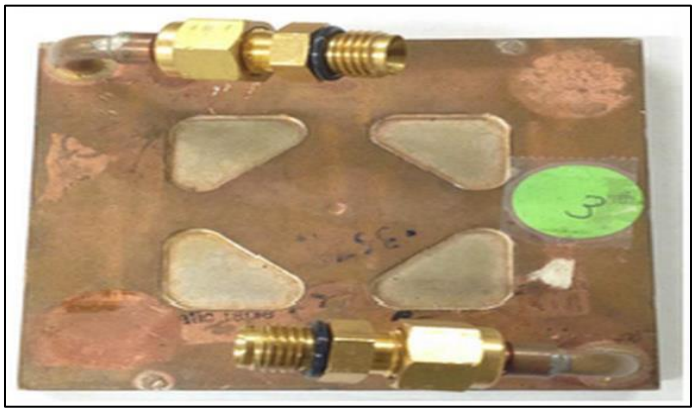

FIGURE 1: COLD PLATE GEOMETRY [5]

The high specific heat capacity of dielectric fluids, being 1100-1200 times greater than that of air, eliminates hot spots and even temperature profile, and they can absorb and store more energy due to their high thermal mass [11] - [13]. Improvement in the immersion cooling method for better thermal performance and substantial energy savings are being tested by using nanofluids, with the size of the nanoparticles of 1 to 150 nanometres. Due to the poor thermal conductivities of traditional heat transfer fluids such as water, oil, and ethylene glycol mixture, adding nano-particles in appropriate concentrations increases the thermal conductivity of the fluid. Metals in solid form exhibit larger thermal conductivity than fluid by orders of magnitude. For example, the thermal conductivity of copper is 3000 times greater than the thermal conductivity of water at room temperature. To keep the dielectric feature of the liquid, oxides of metal such as Al2O3, having larger magnitudes of thermal conductivities compared to water, can be added to base fluids for immersion cooling. Superior heat transfer properties are expected to be exhibited by nanofluids compared to the conventional base fluids. Since heat transfer occurs at the surface, it is desirable to use particles with a large surface area. The large surface area of nanoparticles should improve the heat transfer capabilities, with enhancement in the stability of the suspension [14].

FIGURE 2: IMMERSION COOLED SERVER [15]

Rea et al. [16] reported enhancement in the heat transfer coefficient at 6 vol% alumina nanofluid compared to water in the entrance region, with a lower enhancement displayed by zirconia nanofluid. Numerical and experimental analysis of laminar convective heat transfer of TiO2/Water Nanofluid flowing through a uniformly heated circular tube was conducted by Ebrahimnia-Bajestan et al. [17], reporting a maximum increase of 21% in the average heat transfer coefficient at 2.3 vol% of TiO2. Ghale et al. [18] performed a CFD analysis of Al2O3/water nanofluid in a straight and ribbed MHCS resulting in a 16.1% increase in Nu from 1% to 2% in the volume fraction of alumina. Duangthongsuk et al. [19] Observed higher heat transfer coefficient values with the use of TiO2/water as compared to base fluids, with Pak and Cho's correlation agreeing better with the results of experimentation. Hwang et al. [20] Conducted experimentation which showed the good agreement of Darcy friction factor with theoretical results of the friction factor correlation for the single-phase flow (64ReD). Also, an 8% increase in the heat transfer coefficient was reported for Al2O3/Water nanofluid at 0.3% under the fixed Re as compared to that of pure water. Jung et al. [21] measured the friction coefficient of Al2O3 nanofluid of 170 mm diameter, observing the increase in heat transfer coefficient of nanofluids with the base fluid of water and ethylene glycol at a volume fraction of 1.8 volume percent without major friction losses. From the study on nucleate pool boiling heat transfer of TiO2-R141b nanofluids by Trisaksri et al. [22], no significant effect on the nucleate boiling heat transfer of R141b was observed.

About the literature survey on the liquid cooling using nanofluids, results on the numerical analysis of oil immersion cooling using Al2O3 and Mineral Oil on a Winterfell server is documented in the study. The server and its components are modeled using Ansys Icepack. With the help of available theoretical data and equations, mechanical properties of the nanofluid are calculated. The chosen mass concentrations of Al2O3 are 0%, 1%, 3%, and 5%, and its effects on the temperature reduction of the server and its components are tested. Simulations are performed for 3 different heatsink configurations at different inlet temperatures of 25, 35, and 45 °C with volumetric flow rates of 0.5, 1, 2 and 3 LPM to determine the best case to be used for experimental analysis.

2. Numerical Methods

The server used in the current study is the Third Generation Open Compute Server. It consists of two CPUs with a TDP of 65 W each and the heatsinks are mounted on them respectively. The cabinet houses 16 RAM units on either side of the heatsinks with 4 GB memory each. The server has dimensions of (700mm ×170mm×87mm). The two fans that were originally present for air cooling are removed from the current model. The baseline model of the server is designed using ANSYS Icepak as shown in figure 3.

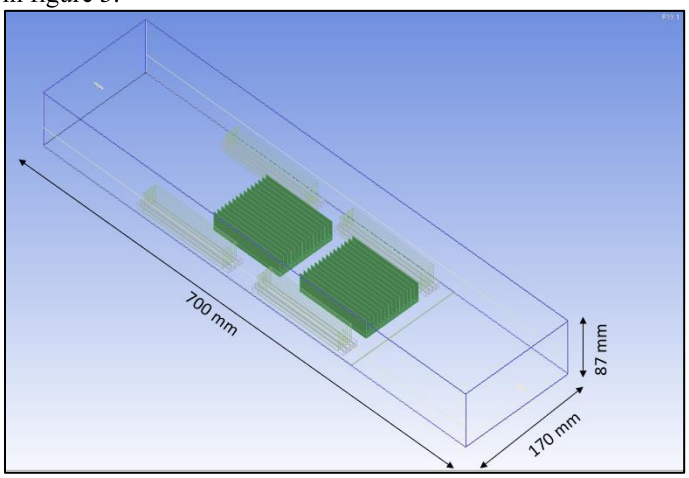

FIGURE 3: BASELINE MODEL OF THE IMMERSION COOLED SERVER

The model incorporates an inlet and outlet in the x-direction. At the inlet of the cabinet, the flow velocity is specified based on the volumetric flow rate, with inlet temperatures varied. Velocities in the y and z directions are assumed to be zero. The outlet is maintained at ambient pressure. Periodic boundary conditions are applied in the z-direction to account for repetitive servers in an experimental setup. The top and bottom walls in the y-direction are maintained at a constant heat flux of $0 W/m^2$. The surroundings have a temperature of 30 °C with a pressure of 1 atm. The boundary conditions are summarized as follows:

Inlet:

u_x = 0.00163, 0.00326, 0.00652 and 0.00978 m/s

$u_y = u_z = 0$

Temperature: 25, 35 and 45 °C

Outlet:

Static Pressure = Ambient (1 atm)

Wall type: Stationary

Heat Flux: $0 W/m^2$

And the rest assumed as periodic boundaries

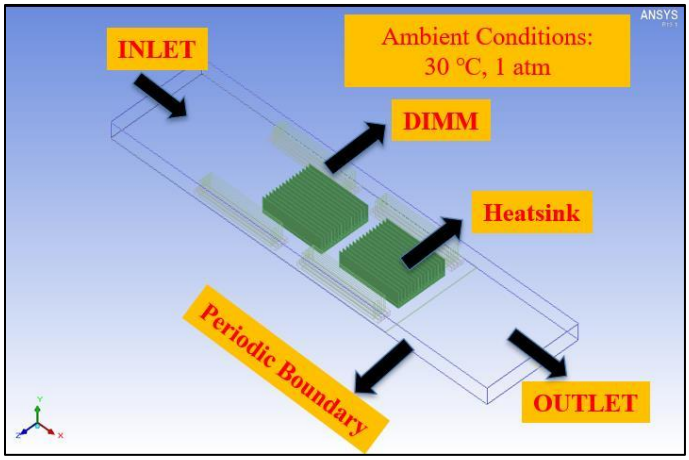

FIGURE 4: BOUNDARY CONDITIONS USED FOR SIMULATION

Physical properties of the nanofluid:

The properties of nanofluid are calculated by the following equations, based on the temperature-dependent properties of pure mineral oil and physical properties of AL2O3, as shown in Table 1 and 2 [23]:

Density: $\rho_{nf} = (1-\emptyset)\rho_f + \emptyset\rho_s$ (1)

Where $\emptyset$ is the mass concentration of Al2O3, ρ_s is the density of Al2O3, ρ_f is the density of pure mineral oil and ρ_{nf} is the density of the nanofluid.

Specific Heat Capacity: $C_{P_{nf}} = \frac{(1-\emptyset)(\rho C_p)_f + \emptyset(\rho C_p)_s}{\rho_{nf}}$ (2)

Where C_{pf} is the specific heat of pure mineral oil, and $C_{P_{nf}}$ is the specific heat of the nanofluid.

Viscosity: $\mu_{nf} = \mu_f(1-\emptyset)^{-2.5}$ (3)

Where μ_f is the viscosity of pure mineral oil and μ_{nf} is the viscosity of the nanofluid.

Thermal Conductivity: $K_{nf} = K_f[\frac{K_s+2K_f-2\emptyset(K_f-K_s)}{K_s+2K_f+\emptyset(K_f-K_s)}]$ (4)

Where K_s is the thermal conductivity of Al2O3, K_f is the thermal conductivity of pure mineral oil, and K_{nf} is the thermal conductivity of the nanofluid.

Thermal Expansion Ratio: $\beta_{T_{nf}} = \frac{(1-\emptyset)(\rho\beta_T)_f + \emptyset(\rho\beta_T)_s}{\rho_{nf}}$ (5)

Where β_{Ts} is the thermal expansion ratio of Al2O3, β_{Ts} is the thermal expansion ratio of Al2O3 and $\beta_{T_{nf}}$ is the thermal expansion ratio of the nanofluid.

TABLE1: PROPERTIES OF PURE MINERAL OIL

Temperature °C	ρ_f Kg/m3	C_{pf} J/Kg-K	μ_f Kg/m-s	K_f W/m-k	β_{Tf}
25	867	1940.04	0.0197	0.133	0.00075
40	857	1990.25	0.01119	0.13	0.00076
60	845	2064.78	0.006355	0.128	0.00078
80	832	2140.68	0.004111	0.126	0.0008

Thermal conductivity and specific heat at different concentrations:

From equations 2 and 4, thermal conductivity and specific heat at various concentrations of Al2O3 are calculated. The physical properties of Al2O3 are shown in Table 2.

TABLE 2: PHYSICAL PROPERTIES OF AL2O3 [24]

Physical Properties	Al2O3
C_p (W/m-k)	765
ρ (Kg/m^3)	3970
K (W/m-k)	40
$\alpha \times 10^7$ (m^2/s)	131.7
β ($K^{-1} \times 10^{-6}$)	8.5

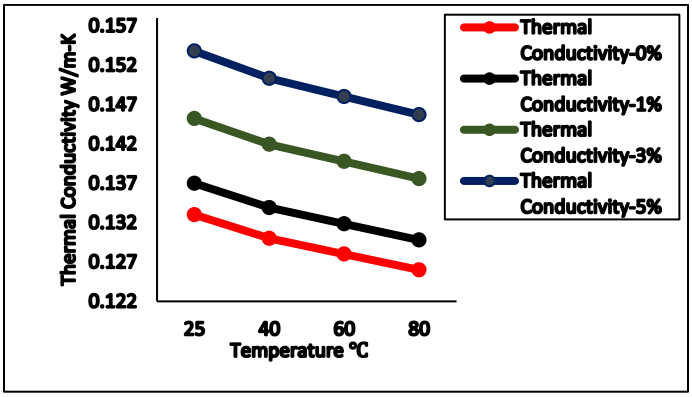

FIGURE 5: VARIATION OF THERMAL CONDUCTIVITY WITH TEMPERATURE AT 0 AND 5 MASS % OF AL2O3

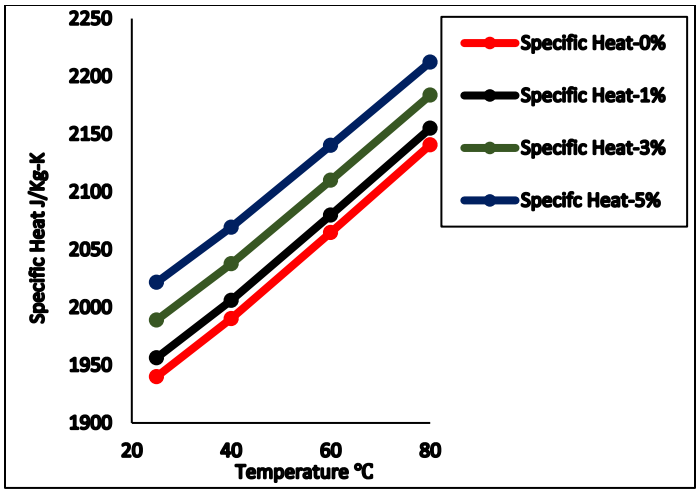

FIGURE 6: VARIATION OF SPECIFIC HEAT WITH TEMPERATURE AT 0 AND 5 MASS % OF AL2O3

Graphs are plotted to study the trends in thermal conductivity and specific heat with nanoparticle mass% concentration and temperature. Figures 5 and 6 show the variation of thermal conductivity and specific heat with temperature, at 0, 1, 3, and 5 mass% of Al2O3 nanoparticles. The maximum increase in thermal conductivity is observed at 5 mass% concentration of Al2O3 and inlet temperature of 25 °C, from an increase of 0.133 to 0.153 W/mK. A decrease in thermal conductivity with temperature is due to the increase in the randomness of molecular movements, obstructing the flow of heat through the liquid. The molecular diffusion effect is more pronounced at higher temperatures, manifested in the decrease of thermal conductivity from 0.153 to 0.145 W/mK at 5 mass% concentration, between 25 and 45 °C inlet temperature.

Also, an increase in nanoparticle concentration from 0 to 5 mass% results in the rise of specific heat, with a maximum enhancement of $C_p = 82\ J/KgK$ observed at 25 °C inlet temperature. At higher temperatures, an increase in specific heat is due to the increase in the average temperature of the nanoparticles, with lesser enhancement in the specific heat between 0 and 5 mass% Al2O3 concentration. Thermal conductivity and specific heat of the fluid at 40 °C at different concentrations are shown in table 3.

TABLE 3: THERMAL CONDUCTIVITY AND SPECIFIC HEAT AT 40 °C

Thermal Conductivity (W/m-K)	Specific Heat (J/Kg-K)	Concentration (%)
0.13	1990.25	0
0.133901	2006.08	1
0.141941	2037.73	3
0.150317	2069.39	5

The flow is assumed to be laminar due to Re<<<230. Ansys Icepak solves the Navier-Stokes equation on the conservation of mass, momentum, and energy, with the specified parameters and boundary conditions. The governing equations solved for simulations are as follows:

$$\frac{\partial \rho}{\partial t} + \nabla.(\rho\vec{v}) = 0 \quad (6)$$

For an incompressible flow, equation (6) reduces to:

$$\nabla.\vec{v} = 0 \quad (7)$$

$$\frac{\partial(\rho\vec{v})}{\partial t} + \nabla.(\rho\vec{v}\vec{v}) = -\nabla p + \nabla.(\bar{\bar{\tau}}) + \rho\vec{g} + \vec{F} \quad (8)$$

Where p is the static pressure, $\bar{\bar{\tau}}$ is the stress tensor, and $\rho\vec{g}$ is the gravitational body force. $\vec{F}$ May arise from resistances, sources and so on ([22]).

$$\frac{\partial(\rho h)}{\partial t} + \nabla.(\rho h\vec{v}) = -\nabla.[(k + k_t)\nabla T + S_h \quad (9)$$

Where k is the molecular conductivity, k_t is the conductivity due to turbulent transport and S_h includes the defined volumetric sources

Mesh sensitivity analysis:

From the graph shown on the maximum CPU temperature v/s the maximum no of elements in the model in Figure 7, the maximum CPU temperature remained nearly constant after an element count of around 1.1 million. For the rest of the study, no of Elements was in the range of 1.1 to 1.9 million elements. The graph was obtained for a flow rate of 0.5 LPM of pure mineral oil.

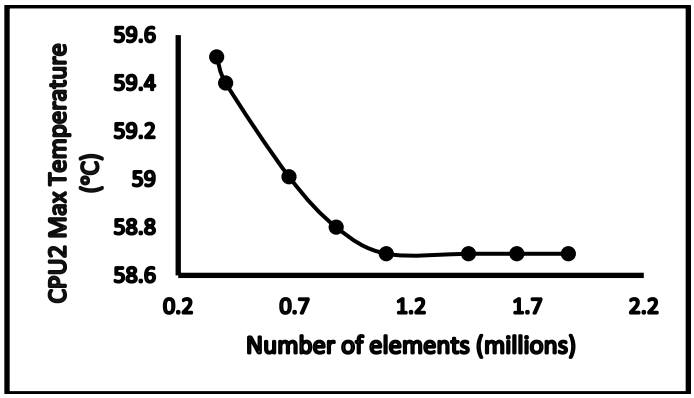

FIGURE 7: MESH SENSITIVITY ANALYSIS

3. RESULTS AND DISCUSSIONS:

Effect of cabinet height on CPU temperature:

Before the study, two simulations were conducted using pure mineral oil at 0.5 LPM to test the effect of cabinet height on CPU temperature. Heights of 87 mm and 30 mm were chosen and a 34% reduction in temperature was observed after stimulation. This is shown by the velocity contours that a larger frame height offers the least resistance above the heatsinks for the fluid flow. On the contrary, smaller cabinet height regulates the fluid to flow through the heatsinks, enhancing the reduction in CPU temperatures. The cabinet height is maintained at 30 mm for the rest of the numerical analysis. The velocity contours for the two simulations are displayed in Figures 8 and 9 respectively.

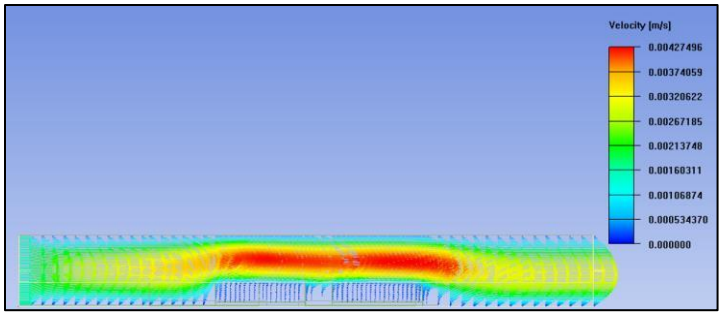

FIGURE 8: VELOCITY PROFILE WITH STANDARD FRAME HEIGHT

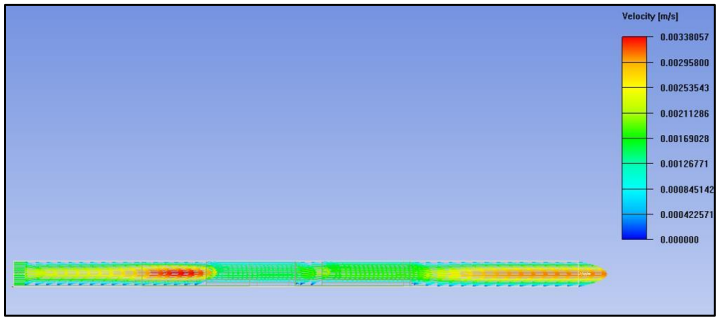

FIGURE 9: VELOCITY PROFILE WITH REDUCED FRAME HEIGHT

Graphs between max CPU temperature, pressure drop, and pumping power at chosen nanoparticle concentrations are plotted against volumetric flow rates for the three heatsink geometries to study the effect of nanoparticle concentration on these parameters.

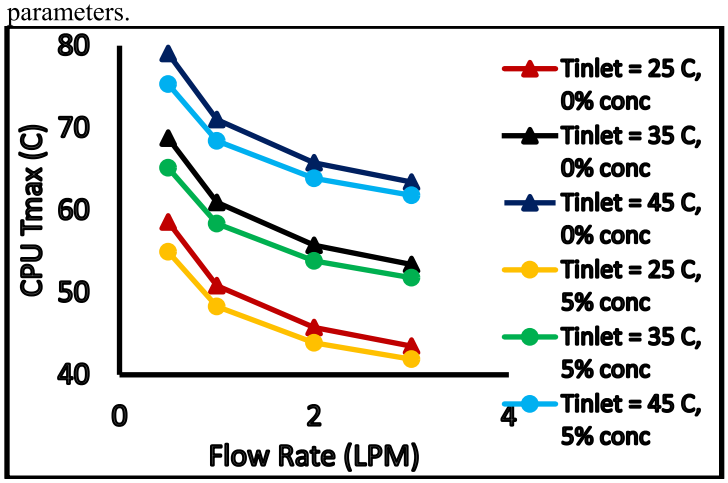

FIGURE 10: VARIATION OF CPU Tmax WITH FLOW RATE AT 0 AND 5 MASS % OF AL2O3 FOR PARALLEL PLATE HEATSINK CONFIGURATION

Figure 10 shows the effect of nanoparticle concentration on the reduction of maximum CPU temperature with the flow rate at three different inlet temperatures. The maximum CPU temperature decreases exponentially with flow rate, from a maximum temperature of 58.58 °C at 0.5 LPM to 43.48 °C at 3 LPM at 0 mass% Al2O3 concentration. By studying the above trends, a reduction in the maximum CPU temperature is observed by increasing the mass% of Al2O3 from 0 to 5%. The highest reduction of 3.72 °C is observed at a 0.5 LPM flow rate and 45 °C inlet temperature, where the maximum CPU temperature reduces from 79.04 to 75.32 °C. However, to maintain the CPU temperature below the 70 °C thresholds, a lower inlet temperature of the nanofluid must be used, ensuring safe and longer operation of the CPU. A maximum reduction in CPU temperature is obtained at 25 °C inlet temperature and 0.5 LPM flow rate, with a reduction of 3.63 °C. Larger flow rates can reduce the maximum CPU temperature further, also causing an increase in pressure drop. Hence the effect of nanoparticle concentration and flow rate on the pressure drop is studied and explained in figure 11.

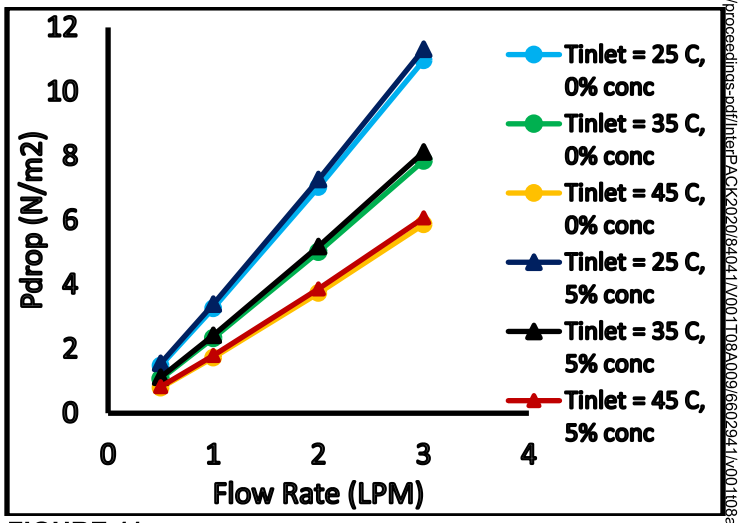

FIGURE 11: VARIATION OF CPU Pdrop WITH FLOW RATE AT 0 AND 5 MASS % OF AL2O3 FOR PARALLEL PLATE HEATSINK CONFIGURATION

Figure 11 shows the increase in pressure drop with flow rate, at inlet temperatures of 25, 35, and 45 °C at 0 and 5 mass% of Al2O3. Maximum pressure of 11.32 N/m2 is observed at 3 LPM flow rate and 5 mass% Al2O3 concentration. With an increase in inlet temperature, pressure drop significantly reduces, where a maximum reduction of 5.25 N/m2 occurs between 45 and 25 °C inlet temperature at 3 LPM flow rate. With an increase in nanoparticle concentration, the fluid tends to become more viscous, increasing the pressure drop. At 25 °C inlet temperature and 0.5 LPM flow rate, minute increase in pressure drop of only 0.075 N/m2 is observed between 0 and 5 mass% Al2O3, as opposed to a 0.351 N/m2 increase at 3 LPM. An increase in flowrate beyond 1 LPM augments pressure drop to values of 7.03 and 10.97 N/m2, thereby increasing the pumping power. The effects of pressure drop on the pumping power are studied, shown in figure 12. From the obtained pressure drop, pumping power is calculated for 0 and 5 mass% of Al2O3 at varying flow rates, for inlet temperatures of 25, 35 and 45 °C using the following relation:

$$P = Q \times \Delta p \quad (10)$$

Where P is the pumping power and Δp is the pressure drop.

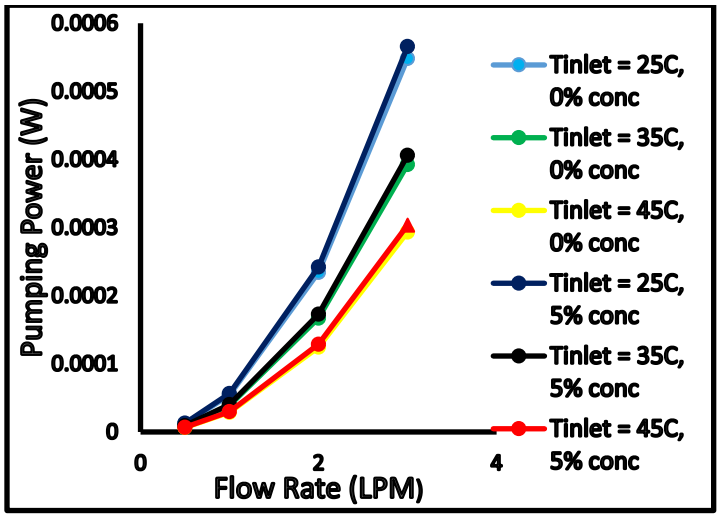

FIGURE 12: VARIATION OF CPU PUMPING POWER WITH FLOW RATE AT 0 AND 5 MASS% OF AL2O3 FOR PARALLEL PLATE HEATSINK CONFIGURATION

From the graph shown in figure 12, no significant increase in pumping power is observed with an increase in nanoparticle mass concentration from 0 to 5%. At 0.5 and 1 LPM, an increase in pumping power of 0.0375 and 0.133 W is obtained at 25 ℃ inlet temperature. The maximum pumping power of 36.96 W is attained at 5% nanoparticle mass concentration and 3 LPM. Hence, to maintain the lower temperature of the CPU's and reduced pumping power, a flow rate of 1LPM and 5% nanoparticle mass concentration are the most ideal conditions of operation.

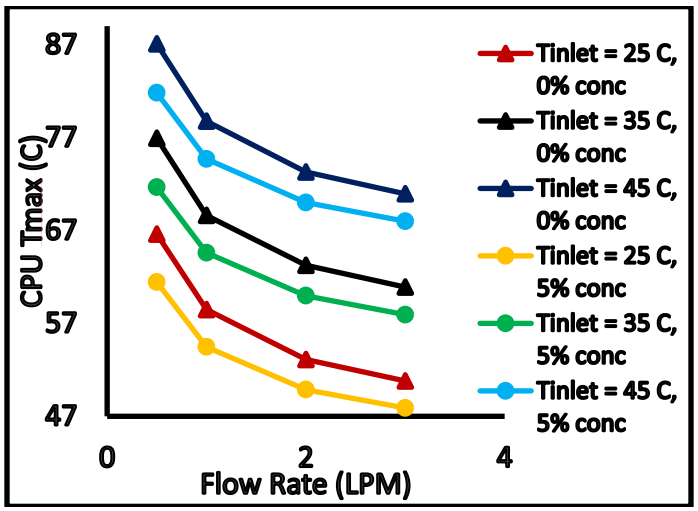

FIGURE 13: VARIATION OF CPU Tmax WITH FLOW RATE AT 0 AND 5 MASS % OF AL2O3 FOR PIN FIN HEATSINK CONFIGURATION

Figure 13 shows the reduction in CPU temperature with the flow rate at 0 and 5 vol% nanoparticle concentration for the pin fin heatsink geometry. A maximum increment in temperature to 87.08 ℃ is observed at 45 ℃ inlet temperature and 0.5 LPM flow rate. The CPU temperature lessens with nanoparticle concentration, with the least temperature of 47.89 ℃ seen at 3 LPM flow rate and 5 mass% nanoparticle concentration, at 25 ℃ inlet temperature, where the maximum CPU temperature reduces by 2.91 ℃. However, to maintain the safe working of the server, pressure drop should be within the safe working limits. At 1 LPM and 25 ℃ inlet temperature, a maximum CPU temperature of 61.45 ℃ is seen, at 5 mass% nanoparticle concentration. To test the safe operating conditions, a study on the effect of nanoparticle concentration and flow rate on the pressure drop is conducted and shown in figure 14.

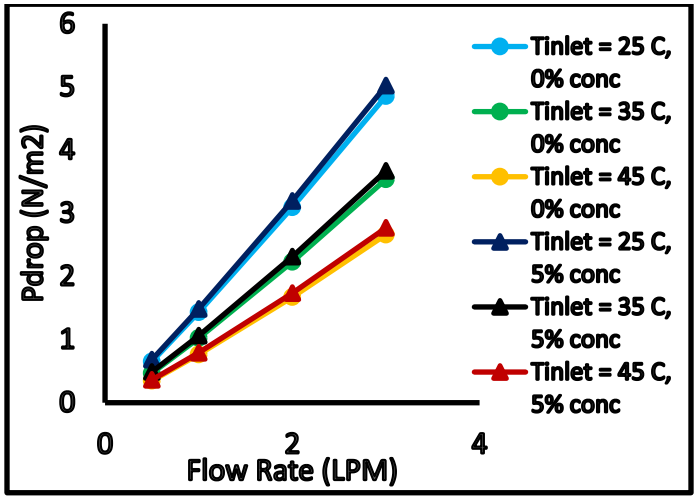

FIGURE 14: VARIATION OF CPU Pdrop WITH FLOW RATE AT 0 AND 5 MASS % OF AL2O3 FOR PIN FIN HEATSINK CONFIGURATION

As shown in figure 14, the least increment of 0.031 and 0.053 N/m2 is seen with nanoparticle concentration at 0.5 and 1 LPM flow rate, at 25℃ inlet temperature. This reduction is more pronounced at higher inlet temperatures of 35 and 45 ℃ inlet temperatures, with 0.021 and 0.015 N/m2 at 0.5 LPM, and 0.038 and 0.028 N/m2 at 1LPM. The pressure drop reaches a maximum value of 5.02 N/m2 at 5 mass% nanoparticle concentration at 3 LPM and 25 ℃ inlet temperature, as opposed to that of the parallel plate heatsink configuration, where the maximum pressure drop reaches 11.32 N/m2. Hence, higher flow rates can be applied using the pin fin heatsink configuration, by decreasing the maximum CPU temperature to a minimum value. At higher inlet temperatures, the pressure drop is further reduced, with 3.67 and 2.76 N/m2 obtained at 35 and 45 ℃, and 3 LPM flow rate. The effects of pressure drop and nanoparticle concentration on the pumping power are studied, as depicted in figure 14.

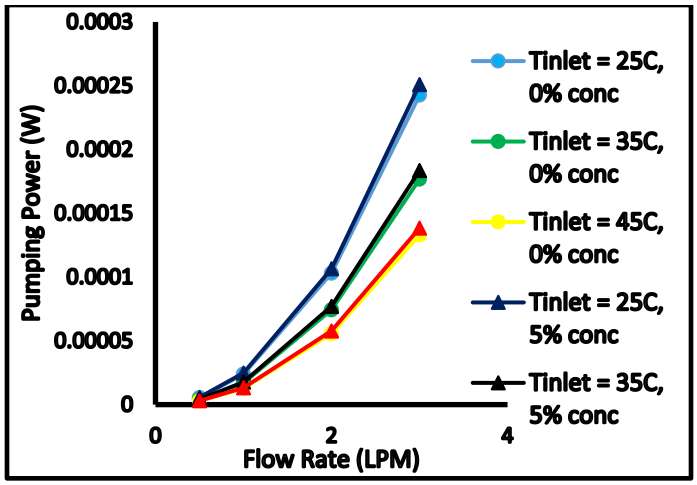

FIGURE 15: VARIATION OF CPU PUMPING POWER WITH FLOW RATE AT 0 QAND 5 MASS % OF AL2O3 FOR PIN FIN HEATSINK CONFIGURATION

Figure 15 shows the effects of nanoparticle concentration and flow rate on the pumping power. Increase in flow rate results in an increase in pumping power. However, the maximum pumping power using the pin fin configuration is much lesser than the pumping power obtained, using the parallel plate heatsink configuration. A maximum pumping power of 15.06 W is observed at 3 LPM and 5 mass% nanoparticle concentration. An increase in inlet temperature reduces the pumping power of operation, with a reduction from 15.06 W to 8.30 W at 3 LPM and 5 mass% nanoparticle concentration. Considering the maximum CPU temperature, 5 mass% nanoparticle concentration at a flow rate of 1 LPM, at an inlet temperature of 25 ℃, resulting in the maximum CPU temperature of 54.46 ℃ are the most ideal parameters for operation, ensuring safe working of the server and reducing the maximum CPU temperature.

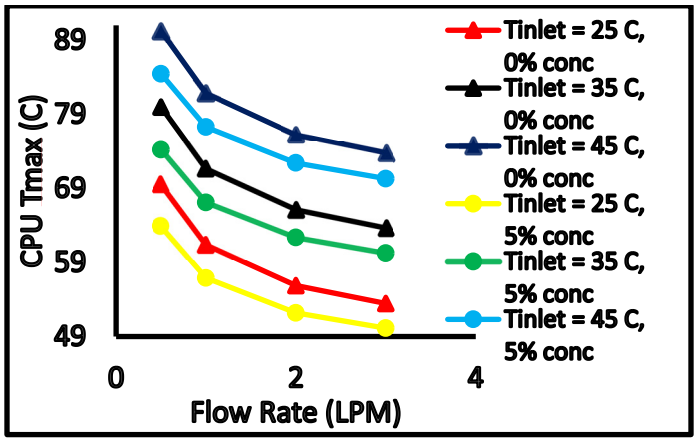

FIGURE 16: VARIATION OF CPU Tmax WITH FLOW RATE AT 0 AND 5 MASS % OF AL2O3 FOR PLATE FIN HEATSINK CONFIGURATION

Figure 16 shows the plot between the maximum CPU temperature and flow rate for 25, 35, and 45 ℃ inlet temperatures at 0 and 5 mass% nanoparticle concentrations, for the plate-fin heatsink geometry. The highest CPU temperature of 90.23 ℃ is seen at 45 ℃ inlet temperature and 0 mass% concentration of Al2O3. At a low inlet temperature of 25 ℃, lower maximum CPU temperatures are obtained, with a maximum reduction of 5.61 and 4.47℃ at flow rates of 0.5 and 1 LPM, between 0 and 5 mass% nanoparticle concentration. To employ the ideal condition of operation, the effects of nanoparticle concentration on the pressure drop and pumping power with flow rates are conducted.

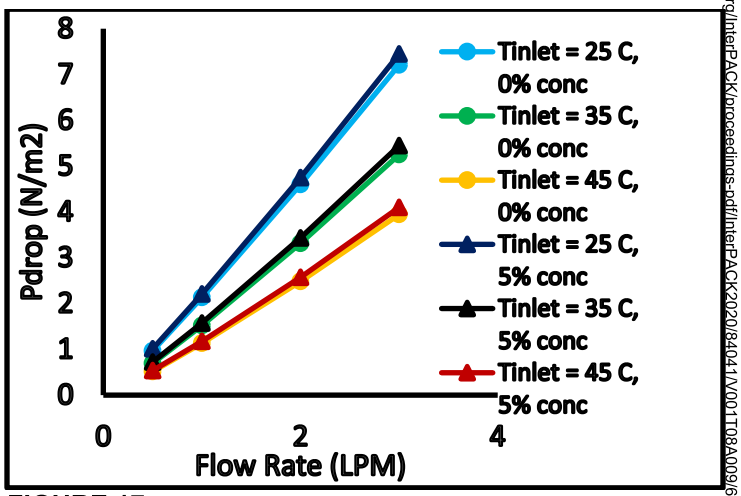

FIGURE 17: VARIATION OF CPU Pdrop WITH FLOW RATE AT 0 AND 5 MASS % OF AL2O3 FOR PLATE FIN HEATSINK CONFIGURATION

Figure 17 shows the plot of pressure drop v/s flow rate for inlet temperatures of 25, 35, and 45 ℃ at 0 and 5 mass% nanoparticle concentrations. A maximum pressure drop of 7.44 N/m2 is seen at 3 LPM flow rate and 5 mass% nanoparticle concentration. An increase in inlet temperature from 25 to 45 ℃ decreases the pressure drop to 4.09 N/m2, at 5 mass% nanoparticle concentration. However, to maintain the low maximum CPU temperature, a lower inlet temperature of 25 ℃ is ideal for operation. Least enhancements in the pressure drop of 0.022 and 0.04 N/m2 is seen at 0.5 LPM and 1 LPM, with lower values of pressure drop maintained, even at 5 mass% nanoparticle concentration.

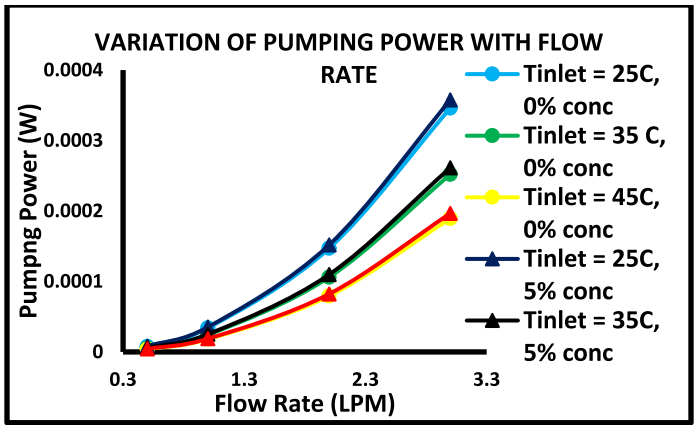

FIGURE 18: VARIATION OF CPU PUMPING POWER WITH FLOW RATE AT 0 AND 5 MASS % OF AL2O3 FOR PLATE FIN HEATSINK CONFIGURATION

As shown in figure 18, pumping power is maintained at lower values of 0.26 and 1.17 W, at 0.5 and 1 LPM flow rates, 5 mass% concentration of Al2O3, and 25 ℃ inlet temperature. Pumping power increases by only 0.003 and 0.04 W between 0 and 5 mass% nanoparticle concentration at this corresponding inlet temperature. Hence, a flow rate of 1 LPM, at 5 mass% Al2O3 concentration, at 25 ℃ inlet temperature results in the lower CPU temperatures, maintaining safer working of the server.

4. CONCLUSIONS:

immersion cooling of Winterfell servers was studied numerically using nanofluid (mineral oil + Al2O3) for different concentrations of Al2O3 at different inlet temperatures of 25, 35 and 45 °C. our findings show that due to the high viscosity of mineral oil, pressure drop and pumping dramatically increases by increasing the flowrate. The pressure-drop and pumping power decreased by increasing the inlet temperature from 25 °C to 35 and 45 °C. Maximum temperature can be reduced by at least 6 °C by increasing the flowrate from 1 LPM to 3 LPM, however the pressure-drop increases by 300%. Therefore, a flow rate of 1 LPM is recommended for cooling. By adding the nanoparticles, the temperature reduces by about 3.5 °C while the pressure-drop increases by just 4%. Amongst the simulated geometries, pin fin heat sink has the lowest pumping power (50% lesser compared to the parallel plate heat sink). Adding nanoparticles can increase pumping power by around 4.4%, however, it can add 7% more capacity to remove heat. Hence using the pin fin heatsink geometry at 1 LPM with 5 percent concentration of Al2O3 in mineral oil at 25 °C for cooling is the most efficient solution for the safe operation of the server and optimum power.

4. REFERENCES:

[1] J. M. Shah, C. Bhatt, P. Rachamreddy, R. Dandamudi, S. Saini, and D. Agonafer, "Computational form factor study of a 3rd generation open compute server for single-phase immersion cooling," 2019, doi: 10.1115/IPACK2019-6602.

[2] P. A. Shinde *et al.*, "Experimental analysis for optimization of thermal performance of a server in single phase immersion cooling," 2019, doi: 10.1115/IPACK2019-6590.

[3] J. M. Shah *et al.*, "Development of a technique to measure deliquescent relative humidity of particulate contaminants and determination of the operating relative humidity of a data center," 2019, doi: 10.1115/IPACK2019-6601.

[4] G. Thirunavakkarasu, S. Saini, J. Shah, and D. Agonafer, "Air flow pattern and path flow simulation of airborne particulate contaminants in a high-density data center utilizing airside economization," 2018, doi: 10.1115/IPACK2018-8436.

[5] "Server immersion cooling," [Online]. Available: https://en.wikipedia.org/wiki/Server_immersion_cooling.

[6] D. Gandhi *et al.*, "Computational analysis for thermal optimization of server for single phase immersion cooling," 2019, doi: 10.1115/IPACK2019-6587.

[7] P. V. Bansode *et al.*, "Measurement of the Thermal Performance of a Custom-Build Single-Phase Immersion Cooled Server at Various High and Low Temperatures for Prolonged Time," *J. Electron. Packag.*, vol. 142, no. 1, Mar. 2020, doi: 10.1115/1.4045156.

[8] S. Ramdas, P. Rajmane, T. Chauhan, A. Misrak, and D. Agonafer, "Impact of immersion cooling on thermo-mechanical properties of PCB's and reliability of electronic packages," 2019, doi: 10.1115/IPACK2019-6568.

[9] B. Kanimozhi and B. R. R. Bapu, "Experimental study of thermal energy storage in solar system using PCM," in *Advanced Materials Research*, 2012, vol. 433–440, pp. 1027–1032, doi: 10.4028/www.scientific.net/AMR.433-440.1027.

[10] R. Eiland, J. Fernandes, M. Vallejo, D. Agonafer, and V. Mulay, "Flow Rate and inlet temperature considerations for direct immersion of a single server in mineral oil," in *Thermomechanical Phenomena in Electronic Systems - Proceedings of the Intersociety Conference*, Sep. 2014, pp. 706–714, doi: 10.1109/ITHERM.2014.6892350.

[11] P. E. Tuma, "The merits of open bath immersion cooling of datacom equipment," in *Annual IEEE Semiconductor Thermal Measurement and Management Symposium*, 2010, pp. 123–131, doi:

10.1109/STHERM.2010.5444305.

[12] P. & M. T. S. Components and Institute of Electrical and Electronics Engineers., *Proceedings of the Fifteenth InterSociety Conference on Thermal and Thermomechanical Phenomena in Electronic Systems : ITherm 2016 : May 31 - June 3, 2016, Las Vegas, NV USA*. .

[13] Bansode, Pratik V., Shah, Jimil M., Gupta, Gautam, Agonafer, Dereje, Patel, Harsh, Roe, David, and Tufty, Rick. "Measurement of the Thermal Performance of a Single-Phase Immersion Cooled Server at Elevated Temperatures for Prolonged Time." *Proceedings of the ASME 2018 International Technical Conference and Exhibition on Packaging and Integration of Electronic and Photonic Microsystems*. San Francisco, California, USA. August 27–30, 2018. V001T02A010. ASME.

[14] S. Lee, -S Choi, S. Li, and J. A. Eastman, "Measuring Thermal Conductivity of Fluids Containing Oxide Nanoparticles," 1999. [Online]. Available: http://heattransfer.asmedigitalcollection.asme.org/.

[15] J. M. Shah, R. Dandamudi, C. Bhatt, P. Rachamreddy, P. Bansode, and D. Agonafer, "CFD Analysis of Thermal Shadowing and Optimization of Heatsinks in 3rd Generation Open Compute Server for Single-Phase Immersion Cooling." Oct. 07, 2019, doi: 10.1115/IPACK2019-6600.

[16] U. Rea, T. McKrell, L. wen Hu, and J. Buongiorno, "Laminar convective heat transfer and viscous pressure loss of alumina-water and zirconia-water nanofluids," *Int. J. Heat Mass Transf.*, vol. 52, no. 7–8, pp. 2042–2048, Mar. 2009, doi: 10.1016/j.ijheatmasstransfer.2008.10.025.

[17] E. Ebrahimnia-Bajestan, M. Charjouei Moghadam, H. Niazmand, W. Daungthongsuk, and S. Wongwises, "Experimental and numerical investigation of nanofluids heat transfer characteristics for application in solar heat exchangers," *Int. J. Heat Mass Transf.*, vol. 92, pp. 1041–1052, Jan. 2016, doi: 10.1016/j.ijheatmasstransfer.2015.08.107.

[18] Z. Y. Ghale, M. Haghshenasfard, and M. N. Esfahany, "Investigation of nanofluids heat transfer in a ribbed microchannel heat sink using single-phase and multiphase CFD models," *Int. Commun. Heat Mass Transf.*, vol. 68, pp. 122–129, Nov. 2015, doi: 10.1016/j.icheatmasstransfer.2015.08.012.

[19] W. Duangthongsuk and S. Wongwises, "Heat transfer enhancement and pressure drop characteristics of TiO2-water nanofluid in a double-tube counter flow heat exchanger," *Int. J. Heat Mass Transf.*, vol. 52, no. 7–8, pp. 2059–2067, Mar. 2009, doi: 10.1016/j.ijheatmasstransfer.2008.10.023.

[20] K. S. Hwang, S. P. Jang, and S. U. S. Choi, "Flow and convective heat transfer characteristics of water-based Al2O3 nanofluids in fully developed laminar flow regime," *Int. J. Heat Mass Transf.*, vol. 52, no. 1–2, pp. 193–199, Jan. 2009, doi: 10.1016/j.ijheatmasstransfer.2008.06.032.

[21] J. Y. Jung, H. S. Oh, and H. Y. Kwak, "Forced convective heat transfer of nanofluids in microchannels," *Int. J. Heat Mass Transf.*, vol. 52, no. 1–2, pp. 466–472, Jan. 2009, doi: 10.1016/j.ijheatmasstransfer.2008.03.033.

[22] J. Y. Jung, H. S. Oh, and H. Y. Kwak, "Forced convective heat transfer of nanofluids in microchannels," *Int. J. Heat Mass Transf.*, vol. 52, no. 1–2, pp. 466–472, Jan. 2009, doi: 10.1016/j.ijheatmasstransfer.2008.03.033.

[23] A. Niazmand, Fathi Sola, J.Alinejad, F.; Rahimi Dehgolan, F.Investigation of mixed convection in a cylindrical lid driven cavity filled with water-cu nanofluid. *Inventions*, 2019,4,60.

[24] B. G. Dehkordi, S. Fallah, and A. Niazmand, "Investigation of harmonic instability of laminar fluid flow past 2D rectangular cross sections with 0.5-4 aspect ratios," *Proc. Inst. Mech. Eng. Part C J. Mech. Eng. Sci.*, vol. 228, no. 5, pp. 828–839, 2014, doi: 10.1177/0954406213491906.

